Crystal and magnetic structures, magnetic and ferroelectric properties of strontium ferrite partially substituted with In ions

Vitalii Turchenko[a,b,c], V. G. Kostishyn[d], Sergei Trukhanov[b,d,e], Francoise Damay[f], Florence Porcher[f], Maria Balasoiu[a,g], Nicoleta Lupu[h], Bernar Bozzo[i], Ignasi Fina[i], Alex Trukhanov[b,d,e], Janusz Waliszewski[a,j], Katarzyna Recko[j], Silviu Polosan[k]

[a]*Joint Institute for Nuclear Research, 6 Joliot-Curie Str., 141980 Dubna, Russia*
[b]*South Ural State University, 76, Lenin Aven., Chelyabinsk 454080, Russia*
[c]*Donetsk Institute of Physics and Technology named after O.O. Galkin of the NASU, 46 Nauki Ave, 03680, Kiev, Ukraine*
[d]*National University of Science and Technology MISiS, 119049, Moscow, Leninsky Prospekt, 4, Russia*
[e]*SSPA "Scientific and practical materials research centre of NAS of Belarus", 19 P. Brovki str., 220072 Minsk, Belorus*
[f]*Laboratoire Leon Brillouin, UMR12 CEA-CNRS, Bât. 563 CEA Saclay, 91191 Gif sur Yvette Cedex, France*
[g]*Horia Hulubei National Institute for Physics and Nuclear Engineering, Bucharest, Romania*
[h]*National Institute of Research and Development for Technical Physics, Iasi, Romania*
[i]*Institut de Ciencia de Materials de Barcelona-CSIC, Campus de la UAB, Bellaterra 08193, Barcelona, Spain*
[j]*University of Białystok, K. Ciołkowskiego 1L street, 15-245 Białystok, Poland*
[k]*National Institute of Materials Physics, Bucharest-Magurele, Romania*

Abstract

The influence of temperature factor to crystal structure as well as magnetic and electric properties of strontium hexaferrite partially substituted with diamagnetic indium ions has been investigated. Ferroelectric properties have been found out in $SrFe_{11.9}In_{0.1}O_{19}$ compound that contradicts to conventional opinion, which describe its crystal structure within the framework of centrosymmetric space group $P6_3/mmc$ (No. 194). For determination fea-

*Vitalii Turchenko
Email address: turchenko@jinr.ru ()

tures of the crystal structure, which are responsible for ferroelectric properties of strontium hexaferrite, have been carried out neutron diffraction measurements with high resolution in temperature range from 1.5 to 740 K. The analysis of hexaferrite structure has been executed within the framework both centrosymmetric and non- centrosymmetric space group. Values of coefficients of magneto crystalline anisotropy at 5 and 300 K and influence of ambient temperature to linear size of magnetic regions have been determined from magnetic measurements.

Keywords: strontium ferrite, neutron diffraction, spontaneous polarization, crystal structure, magnetic properties

---

1. Introduction

Strontium ferrites M-type and their solid solutions attract much attention due to unique functional properties: large magnetocrystalline anisotropy [1, 2], high values of the Curie temperature (∼740 K) [3, 4], very low electrical conductivity (∼ 10^5 - 10^9 Ohm×cm) [5] and relatively large magnetization [6, 7] and etc. As a result, hexaferrite systems are suitable for use in microwave and millimeter wave devices as permanent magnets [59], in high-density magnetic recording media [9], in magneto-optics [10] and as gyromagnetic materials, e.g., in phase shifters [11], filters [12], isolators [13], inductors [14] and in miniature circulators [15, 16, 17] that can be applied in electronic components for automobile and in wireless communication systems [18]. The electronic pollution produced by gigahertz electronic telecommunication systems is able to influence to electronic systems exciting interruptions in their work. Hexaferrites have large dielectric and magnetic losses in the microwave frequency band [19, 20], therefore, they can be used as microwave absorption devices in GHz range [21, 22].

It is well known that the initial hexaferrite $SrFe_{12}O_{19}$ is isostructural to the $PbFe_{12}O_{19}$ magnetoplumbite, which crystal structure was determined by Adelskold [23] in 1938. There are two formula units (Z = 2) per unit cell of M-type hexagonal ferrite, i.e. the unit cell contains 2 strontium ions, 24 iron and 38 oxygen ions. The closest packing of O^{2-} ions forms several types of voids: octahedra 2a, 12k and $4f_{VI}$; tetrahedra $4f_{IV}$ and trigonal bipyramid 2b, where magnetic iron ions are located. Such a complex unit cell is characterized by significant crystalline anisotropy that is reflected in the ratio of lattice parameters c/a ≈ 3.96.

As a rule, the crystal lattice is described within the framework of the centrosymmetric space group (SG) $P6_3/mmc$ (No. 194) [24, 25]. However, relatively recent studies of the interactions of strontium and barium hexaferrites with electric fields [26, 27], discovered the presence of spontaneous electric polarization, which mechanism of appearance remains controversial. In the initial compounds $MFe_{12}O_{19}$ ($M = Ba; Sr$ or Pb) [26, 27, 28] of hexaferrites, the presence of nonzero spontaneous electric polarization has been explained by the distortion of single oxygen octahedron FeO_6 due to displacement of the iron ion from the center [26, 29]. It was assumed that the distortion of a single oxygen octahedron FeO_6 occurs below the Curie temperature. In solid solutions of hexaferrites partially substituted with diamagnetic ions, such as $BaFe_{12-x-\delta}Sc_xMg_\delta O_{19}$ (x = 1.6; $\delta = 0.05$) [30], the appearance of ferroelectric properties has been explained by the presence of a non-collinear magnetic structure. Moreover, the direct relationship between the electrical and magnetic subsystems has been observed in Ref.[30]. As a result, taking into account a rather high temperature of the phase transition from ferrimagnetic to paramagnetic order allows considering these compounds as promising multiferroics [31]. Similar magnetoelectric materials on the base of hexaferrite systems will be compatible with components based on semiconductors and find technical applications in designing of modern devices such as sensors [32] or converters of magnetoelectric effects [33, 34, 35].

The present work is devoted ascertaining of correlation of diamagnetic substitution in strontium ferrite $SrFe_{11.9}In_{0.1}O_{19}$ with mechanism of appearance of double ferroic properties. In our work, we studied the effect of ambient temperature to crystal and magnetic structures as well as distortions of oxygen octahedrons of strontium ferrite with partial replacement of magnetic iron ions by diamagnetic indium ions. Another feature of our work is application of neutron diffraction methods with both constant wavelength and time-of-flight method in a wide temperature range that allowed obtaining information about evolution for both the crystal and magnetic structures during one experiment.

2. Experimental Procedure

The polycrystalline sample $SrFe_{11.9}In_{0.1}O_{19}$ has been obtained by the solid-state reaction method. The initial oxides Fe_2O_3, In_2O_3 and carbonate $SrCO_3$ have been mixed in appropriate proportions and synthesized at temperature 1200^oC (6 h) in air. The reaction of the initial ions is based on the

thermal diffusion of iron, indium and strontium ions over a concentration gradient. As a result, a phase formation reaction of M-type isostructural hexaferrite occurs:

$$SrCO_3 + 0.05 \cdot Fe_2O_3 + 0.05 \cdot In_2O_3 \rightarrow SrFe_{11.9}In_{0.1}O_{19} + CO_2 \uparrow \quad (1)$$

The resulting composition was pressed and annealed at 1300^oC (6 h) and then slowly cooled ($\sim 100\ ^oC$/h).

The Curie temperature has been determined as the inflection point in the temperature dependence of the specific magnetization, which measured by the ponderomotive method in the temperature range 300 - 800 K under external magnetic field 0.86 T on the equipment, which has been early described in Ref.[36]. Magnetization measurements have been carried out on the MPMSXL superconducting quantum SQUID interferometer in the temperature range from 4 to 300 K.

Temperature dependences of magnetization were measured by zero field cooled (ZFC) and field cooled warming (FCW) methods under applied magnetic field 0 and 100 Oe, respectively.

Ferroelectric loops were measured using TFAnalyser 2000 (Aix-ACCT SystemsGmbH. Co.). The surface of strontium hexaferrite was coated with silver paste electrodes. The polarization has been determined as the integral of current over time.

Neutron diffraction studies of sample in the temperature range from 1.5 to 350 K have been carried out on the diffractometer G 4-1 in a monochromatic neutron beam with a wavelength of 2.426 $\AA$ in the experimental hall of the nuclear center in Laboratoire Leon Brillouin (LLB) (Saclay, France). The measurements have been carried out in a helium cryo refrigerator. Neutron investigation of $SrFe_{11.9}In_{0.1}O_{19}$ sample at 740 K has been carried out on the High Resolution Fourier Diffractometer (HRFD) [37] in experimental hall of pulsed nuclear reactor IBR-2 in Dubna. The Rietveld analysis of neutron diffraction patterns has been carried out by FullProf software package [38].

3. Result and Discussion

3.1. Magnetic properties

The magnetic hysteresis loops of the $SrFe_{11.9}In_{0.1}O_{19}$ compound measured at different temperatures are shown in Fig. 1. The magnitude of saturation specific magnetization σ_s reaches value $\sim$85 emu/g and $\sim$91 emu/g at

300 K and 5 K, respectively, that is comparable with values $M_s \sim 78$ emu/g in Ref.[39, 40, 41].

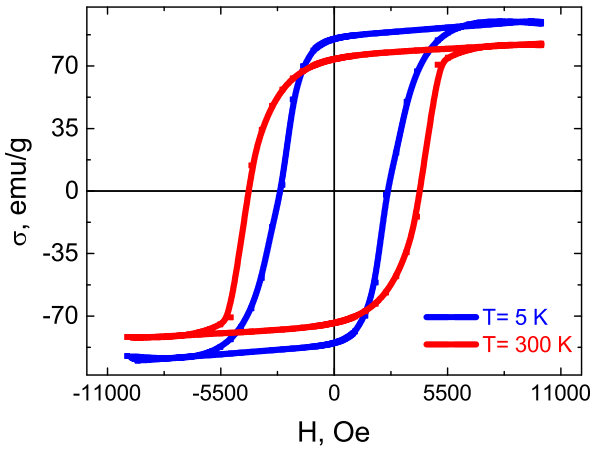

Figure 1: The field dependencies of the specific magnetization $\sigma(H)$ of the $SrFe_{11.9}In_{0.1}O_{19}$ compound measured at 5 and 300 K.

In order to estimate the magneto-crystalline anisotropy constant K of In substituted strontium ferrite, the law of approach to saturation has been used [42, 43]. The field of crystalline anisotropy H_a for uniaxial hexaferrite particles have been evaluated using expressions from Ref. [44, 45, 46]. Values of coercive fields H_c as well as constants of magnetocrystalline anisotropy K that shown in Table.1 are comparable with values $H_c \sim 1$ - 5 kOe [47, 48, 49] and $K \sim 3.6 * 10^6\ erg/cm^3$ [41, 50].

Table 1: The parameters of remanence and saturation magnetization, squareness ratios, constants of magnetocrystalline anisotropy, fields of coercive and crystalline anisotropy

Temperature, K	σ_r emu/g	σ_s emu/g	SQR	$K_{eff} \times 10^6$, erg/cm^3	$H_a \times 10^4$, Oe	H_c, Oe
5	85	91	0.93	3.64	1.539	2560
300	74	85	0.87	2.99	1.371	4185

According to Fig. 1 and Table 1 the value of the coercive field of the $SrFe_{11.9}In_{0.1}O_{19}$ compound reduces in ∼1.6 times from 4185 to 2560 Oe as the ambient temperature is decreased from 300 to 5 K, respectively. The similar behavior of the coercive field has been previously observed in $SrFe_{12}O_{19}$ [51] and $BaFe_{12}O_{19}$ [52] ferrites and it was explained by imperfection of the crystal structure due to its proximity to the amorphous state. The Stoner – Wohlfarth theory [53, 54] makes out polycrystalline ferromagnets as ensemble consisting of weakly interacting monodomain particles with uniaxial anisotropy where homogeneous magnetization of magnetic particles is achieved by the strong interatomic exchange interaction, which exceeds the anisotropy energy in this material. Consequently, the process of reversal magnetization of individual particle is realized by rotation of magnetization vector that changes both anisotropy energy and Zeeman energy in the external magnetic field, while the exchange energy of particle does not change. In that case, the coercive field of material rises with increasing magnetic anisotropy constant and decreases as saturation magnetization is increased, similar to the behavior of the field of crystalline anisotropy described in Ref.[53, 55]. Therefore, the change of coercive field is determined by competition between magnetic anisotropy constant and saturation magnetization. As the result, decreasing of H_c value with decreasing of ambient temperature is explained by the fact that the saturation magnetization rises faster than the magnetic anisotropy constant.

One of the significant characteristics of hexaferrites is the squareness ratio (SQR) of hysteresis loop. SQR is the ratio of residual magnetization to saturation magnetization (σ_r/σ_s), in our case achieves values $\sim$ 0.93 and 0.87 at 5 K and 300 K, respectively, that exceed values 0.5 - 0.67 in Ref.[56, 57, 58]. The significant value of squareness ratio indicates that the particles are single magnetic domain. As a rule, large SQR values are promising for storage devices, where the writing and reading of information is carried out by switching the core from one magnetic state to another because of current pulses, which generate the required magnetic field intensity.

The temperature dependencies of specific magnetization collected in ZFC and FCW modes for $SrFe_{11.9}In_{0.1}O_{19}$ composition are shown in Fig. 2. The values of the phase transition temperature from ferrimagnetic to paramagnetic state are shown in the insert. Less value of the Curie temperature ($\sim$ 670 K) of $SrFe_{11.9}In_{0.1}O_{19}$ ferrite, comparing with the initial compound $SrFe_{12}O_{19}$ ($T_C \sim$ 732 K) [40, 59], confirms the substitution of magnetoactive iron ions by diamagnetic indium ions. Such substitution leads to frustration

of the magnetic structure and destroyed long-range exchange interactions $Fe^{3+} - O - Fe^{3+}$ at lower temperatures. The similar decreasing of T_c value can be attributed with influence not only of indium concentration, but also with the features their distribution in the different oxygen polyhedra that will be investigated with Mossbauer method in our further work.

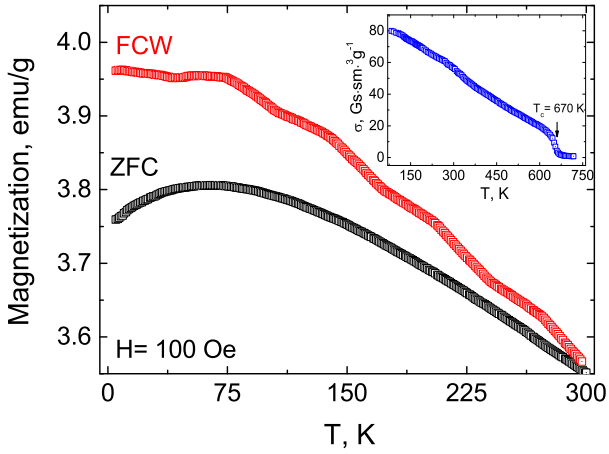

Figure 2: The temperature dependencies of the specific magnetizations of the $SrFe_{11.9}In_{0.1}O_{19}$ hexaferrite received in ZFC and FCW mode. The inset shows the temperature dependence of the specific magnetization with mark of the Curie temperature.

The magnetization curve of ZFC are located lower FCW and first shows growth passing through a maximum and then decreases as the ambient temperature is increased. The difference between ZFC and FCW curves has been previously observed in ensembles of superparamagnetic particles [62], in spin glasses [63], as well as in macroscopic magnets with frustration of exchange bonds, with topological disorder, with structural defects and even in ordered ferromagnets with significant magnetic anisotropy [64]. The decreasing of ambient temperature of weakly interacting uniaxial monodomain particles when the external magnetic field is absent leads to ordering of magnetic moments along easy magnetization axes of crystallites, which are randomly oriented in space. The magnetization of magnetic regions is "frozen" at certain temperature in the process cooling of the sample. Initially, the magnetization of regions with the largest size are frozen at the temperature (T_{irr} = 300 K) of divergence ZFC and FCW curves whereas magnetic moments

of smaller regions, but constituting a significant volume in the sample, are frozen at the blocking temperature (T_b = 55 K). However, the distribution of magnetic moments in crystallites remains chaotic and the total magnetic moment is still zero at the beginning as well as at the end of cooling process. The value of T_b corresponds to the temperature below which the energy of thermal fluctuations in crystallites is significantly less than the energy of magnetic anisotropy and can be expressed by the Bean-Livingston equation [65, 66, 67, 68]:

$$T_B = \frac{K_V V}{25 k_B} \tag{2}$$

The wide maximum on the ZFC curve (Fig.2) indicates the presence of size dispersion of magnetic regions and it is the sum of narrow maxima domains with various sizes. In that way, a wide maximum is determined by the contribution of volume fractions of domains with certain size. The observed maximum on the ZFC curve at 55 K corresponds to the value of average linear size of domain ∼2.3 nm, whereas the maximum linear size of magnetic region, which has been frozen at 300 K has value ∼4.4 nm. In the case of cooling the sample in the external magnetic field (H= 100 Oe), the direction of magnetization in each crystallite is determined by the competition between anisotropy energy and Zeeman energy. The magnetization of crystallites tries to orientate along the external magnetic field, but for rotating magnetic moments into direction corresponding to the minimum energy, it is necessary to overcome the energy barrier:

$$\Delta E \approx K_V \cdot V \tag{3}$$

where K_V is the volume anisotropy constant; V is the volume of magnetic region, which should be overcome by magnetic field in order to change the orientation of the magnetic moment in crystallites. At a sufficiently large value of the external field, magnetic moments of all domains are ordered along the magnetic field. In that case, the shape of temperature dependence curve is determined by increase of spontaneous magnetization of material.

3.2. Ferroelectric properties

The electric voltage dependences of the polarization P for strontium hexaferrite $SrFe_{11.9}In_{0.1}O_{19}$ at room temperature are shown in Fig.3. A rapid increase of the saturation polarization of strontium ceramic is increased under electric field. The presence of hysteresis loops and appearance of remanent

electrical polarization at room temperature that can be reversed by the application of an external electric voltage allows characterize strontium ferrite as ferroelectric. The maximal values of polarization (P_{max}) and spontaneous polarization (P_r) as well as the coercive force (E_C) determined from the hysteresis loops have the following values: 4.17 nC/cm^2, 1.35 nC/cm^2 and 138 V, respectively. It is necessary to note that less magnitudes of spontaneous polarization in our case comparing with earlier discovered in initial compound $SrFe_{12}O_{19}$ [27] can be explained by less values of electric voltage applied in our experiment.

Nevertheless, the mechanism of appearance of ferroelectric properties in solid solutions of hexaferrites remains controversial, because all previous investigations [26, 27, 28, 30] did not paid enough attention to analysis of the complex crystal structure of these materials. Probably, a key role in appearance of ferroelectric properties in hexaferrites should belong to features their crystal structure as was assumed in Ref.[69]. As was mentioned above, the main reason of generation of ferroelectric properties in the initial compounds $AFe_{12}O_{19}$ (where A = Pb, Ba, Sr) [26, 27, 28] has been explained by distortion one of the oxygen octahedra, while in Ref. [30] the origin of spontaneous polarization was associated with occurrence of a non-collinear magnetic structure. In our opinion, the appearance of ferroelectric properties in the $SrFe_{11.9}In_{0.1}O_{19}$ compound is a consequence of non-centrosymmetric distortion its unit cell [70, 71] that will be discussed below.

3.3. Crystal structure

According to analysis of neutron patterns of $SrFe_{11.9}In_{0.1}O_{19}$, which shown in Fig. 4, sample is homogeneous. The presence of thin and well-resolved diffraction peaks indicates the formation of a high-quality crystalline structure. As was mentioned above, the crystal structure of hexaferrites is usually described within the framework of SG 194 [59, 60, 61]. However, this space group has an inversion center and is centrosymmetric that contradicts to the appearance of ferroelectric properties in $SrFe_{11.9}In_{0.1}O_{19}$ shown in Fig.3. In order to remove this contradiction it was proposed to describe the crystal structure of hexaferrites in the framework of non-centrosymmetric space group $P6_3mc$ (No. 186) [69], but no information about atomic coordinates or lattice parameters for this unit cell were given. Therefore, to clarify the real crystal structure of the $SrFe_{11.9}In_{0.1}O_{19}$ compound the high-resolution neutron diffraction data have been collected in a wide temperature range from 1.5 to 740 K that are shown in Fig. 4 and 5. Experimental points

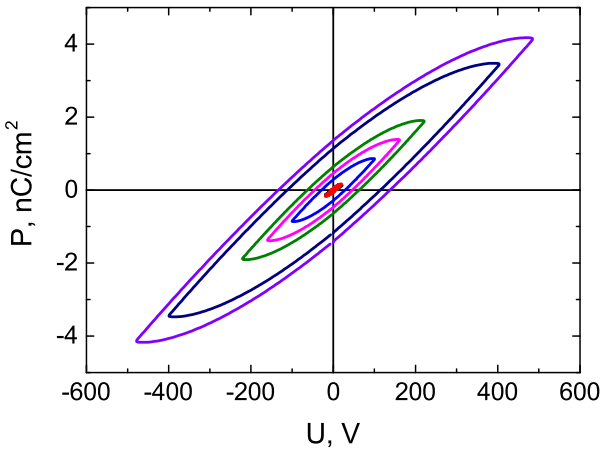

Figure 3: Ferroelectric hysteresis loops of $SrFe_{11.9}In_{0.1}O_{19}$ ceramic.

and calculated curves, as well as the difference function normalized to the statistical error are shown. Vertical bars indicate the calculated positions of the diffraction peaks for the crystalline (top) and magnetic (bottom) structures of strontium hexaferrite. The refinement of crystal structure of the $SrFe_{11.9}In_{0.1}O_{19}$ compound has been carried out in the framework of the centrosymmetric $P6_3/mmc$ (No. 194) and non-centrosymmetric $P6_3mc$ (No. 186) space groups. Results of refinement are shown in Tables 2 and 3.

The comparison of magnitudes figures of merit (R_{exp}, R_{wp}, χ^2) indicates that the crystal structure of strontium hexaferrite can be described quite well by both space groups in a wide temperature range. However, figures of merit for non- centrosymmetric space group have a little bit less values than for centrosymmetric (see Table 2 and 3). Therefore, observation of ferroelecric properties in the $SrFe_{11.9}In_{0.1}O_{19}$ compound shown in Fig.3 and lower magnitudes figures of merit in the case of non-centrosymmetric space group allows us to give preference to SG $P6_3mc$ (No. 186).

The temperature dependences of lattice parameters (a and c) and the volume of unit cell (V) are shown in Fig.6. It is necessary to note that lattice

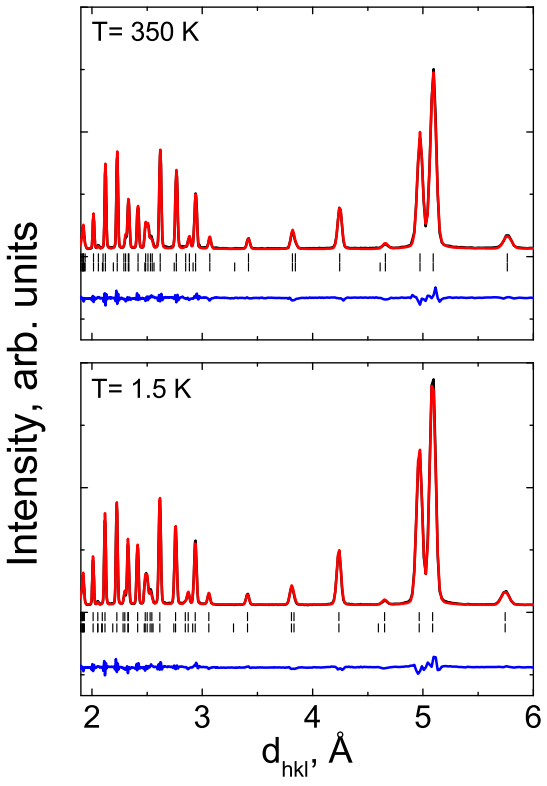

Figure 4: Neutron diffraction patterns of $SrFe_{11.9}In_{0.1}O_{19}$ compound measured on diffractometer G 4-1 at temperatures 350 – (a) and 1.5 K – (b) and processed in the framework of non-centrosymmetric SG $P6_3mc$ (No. 186) by the Rietveld method.

parameters and volume of unit cell described within the framework both centrosymmetric $P6_3/mmc$ and non-centrosymmetric $P6_3mc$ space groups have the same values (see Fig.6 and Table 2 and 3). In the low-temperature region was observed area where thermal extension of lattice parameters is absent. For the first time, such behavior was discovered in similar solid solutions of barium hexaferrite [72]. There is a difference in the temperature

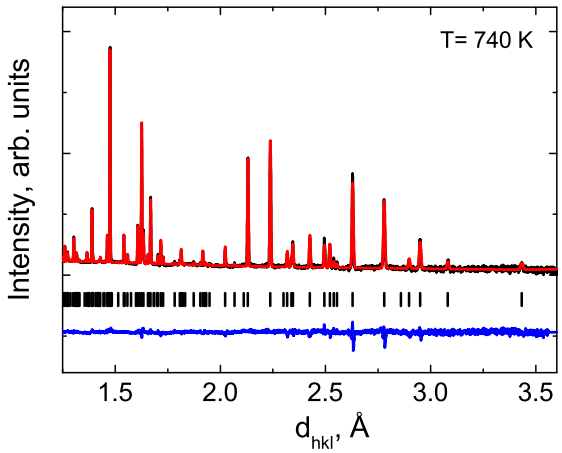

Figure 5: Neutron diffraction pattern of $SrFe_{11.9}In_{0.1}O_{19}$ compound measured on HRFD at 740 K and processed in the framework of centrosymmetric SG $P6_3/mmc$ (No. 194) by the Rietveld method.

dependences of lattice parameters a and c. In particular, c parameter has insignificant variation in the temperature range from 1.5 to 100 K, while a parameter practically does not change in a wider temperature area from 1.5 to 150 K. This difference of changes of unit cell parameters a and c can be related with strong magneto crystalline anisotropy of strontium hexaferrite, while the presence of temperature range where thermal expansion is absent can be explained by mutual rotations and tilts of oxygen polyhedra, similarly to Ref.[72]. Linear and volume coefficients of thermal extension calculated in the temperature range from 150 to 740 K have values $\alpha_a = 7.5 \times 10^{-6}$ 1/K; $\alpha_c = 1.32 \times 10^{-5}$ 1/K and $\alpha_V = 2.83 \times 10^{-5}$ 1/K.

In Fig 7 are shown fragments of the crystal structure of unit cells for centrosymmetric and non-centrosymmetric space groups. Despite the same values of lattice parameters for unit cells both space groups (see Fig. 6 and Tables 2 and 3); it is observed a difference in the distortion of individual structural elements.

For instance, distortions are absent in oxygen octahedra in crystallographic position (2a) Fe1 in the case of description of the unit cell of $SrFe_{11.9}In_{0.1}O_{19}$ hexaferrite with centrosymmetric space group No. 194. Another situation is observed in the case of non-centrosymmetric SG 186, distortions of the same oxygen octahedron reach values $\sim$ 5 - 7 % (see Fig.8 a) in the studied

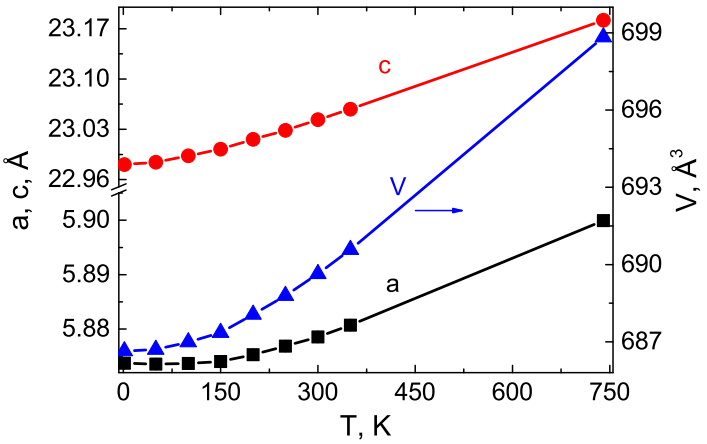

Figure 6: Temperature dependencies of structural parameters a and c (left scale) and volume V (right scale) of unit cell for $SrFe_{11.9}In_{0.1}O_{19}$ compound.

temperature range. In order to evaluate the distortion of oxygen octahedron (S_{FeO_6}) has been used equation:

$$S_{Fe_2O_3}(T) = \frac{100\%}{< d(T) >} \times \sqrt{\frac{\sum_{i=1}^{6}(d_i(T) - < d(T) >)^2}{5}} \qquad (4)$$

where $d_i(T)$ is the distance between the iron ion and the nearest oxygen ion; $< d(T) >$ is the average distance $< Fe - O >$ in the oxygen octahedron. The temperature dependences of oxygen octahedra deformation in the unit cell of $SrFe_{11.9}In_{0.1}O_{19}$ for both No. 194 and 186 space groups are shown in Fig. 8.

According to Ref. [69], the distortion of trigonal bipyramid polyhedron, which placed in crystallographic position (2b) Fe2 of SG 194, has significant contribution to polarization of unit cell in hexaferrites. According to our data distances among iron ion Fe2 and two apical oxygen ions O1 have the same values in a wide temperature range. When the ambient temperature is increased from 1.5 to 350 K, the distances between the $Fe2 - O1$ ions are changed, but equal distances among Fe2 and apical oxygen ions O1 are maintained, as result, the dipole moment in bipyramidal polyhedra will be absent. In the case of non-centrosymmetric SG 186, the interionic distances $Fe2 - O1$ and $Fe2 - O11$ have different values from each other. The effect of

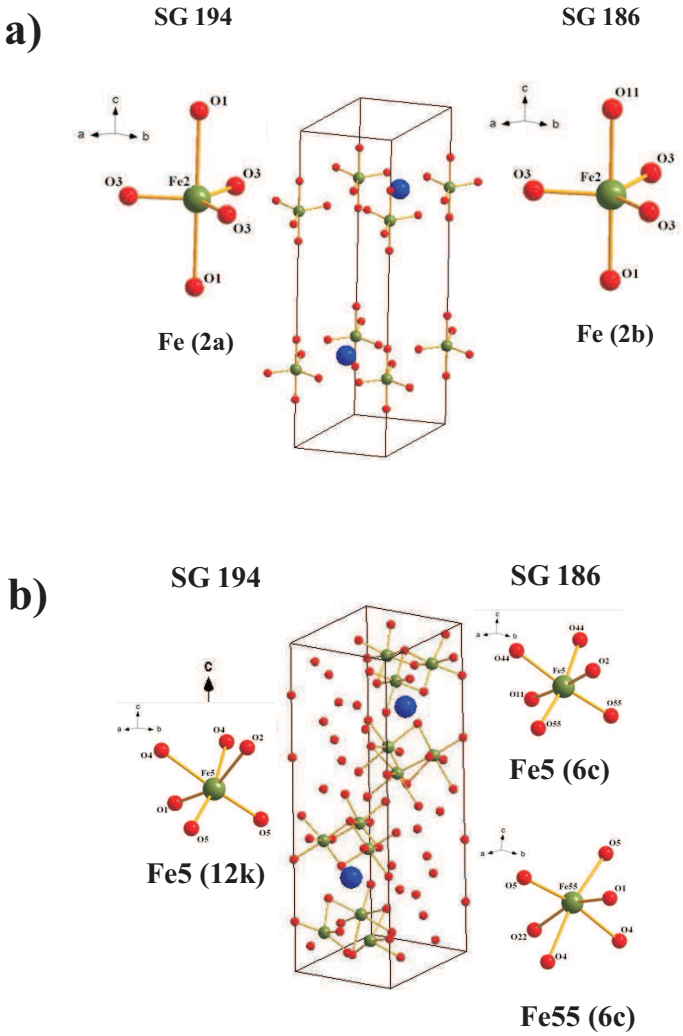

Figure 7: Fragments of unit cell: oxygen polyhedra around Fe2 ion - undistorted for SG 194 and distorted for SG 186 – (a); and oxygen octahedra around Fe5 for SG 194 and around Fe5/Fe55 for SG 186 – (b).

temperature factor to distances $Fe2-O1$ and $Fe2-O11$ is shown at Fig.9. The relative change in distances among iron ion Fe2 and apical oxygen anions O1 and O11 has been estimated as:

$$\frac{\Delta r_{(Fe-O)}}{r_0} = \frac{r_{(Fe2-O11)} - r_{(Fe2-O1)}}{r_{(Fe2-O11)}} \times 100\% \qquad (5)$$

where $r_{(Fe2-O11)}$ – distance between Fe2 and apical anion O11; $r_{(Fe2-O1)}$

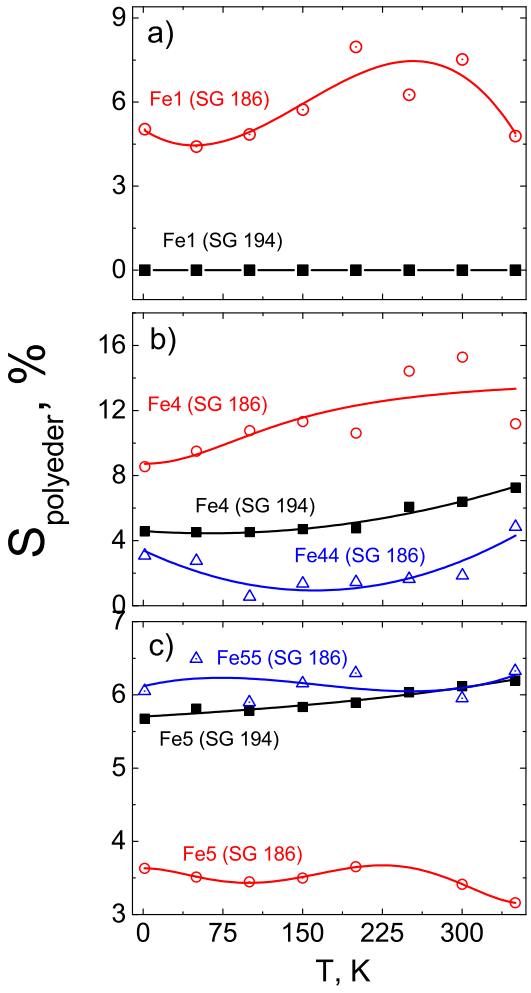

Figure 8: Temperature dependence of distortions of oxygen octahedra in the case of centosymmetric SG $P6_3mc$ (solid squares) and non- centosymmetric SG $P6_3mc$ (open circles and triangles) around: Fe1 ion - (a); and Fe4 and Fe44 ions - (b); and Fe5 and Fe55 ions - (c).

– distance between Fe2 and another apical anion O1. Rising ambient temperature from 1.5 K to 150 K increases distance $Fe2 - O1$ from 2.1786 $\AA$ to 2.2542 $\AA$ and then leads to decreasing distance to value 2.0970 $\AA$ as the temperature is increased up to 300 K unlike of distance $Fe2 - O11$, which decreases from 2.1786 $\AA$ to 2.1392 $\AA$ in temperature range from 1.5 K to 150

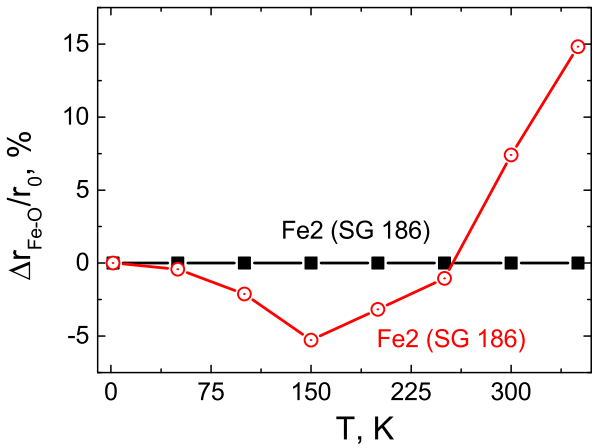

Figure 9: Temperature dependencies of relative changes in distances: between Fe2 and apical oxygen O1 in the case of SG $P6_3/mmc$ - solid square and among Fe2 and apical oxygen ions O1 and O2 in the case of SG $P6_3mc$ - open circles.

K and then increases up to 2.2583 $\AA$ at 300 K. Similar behavior indicates the change direction of electric dipole that is reflected in appearance of negative sign of dipole moment in Fig.10 (b). The change of electric dipole direction occurs along hexagonal c axis. As distinct from oxygen octahedron Fe1 and bipyramid Fe2 others oxygen octahedra in centrosymmetric space group No. 194 have distortions, which values are shown in Fig.8 b and c. For instance, distortions in oxygen octahedra occupying crystallographic positions ($4f_{VI}$) monotonously increase from $\sim$ 5.7 to 6.2 % as the ambient temperature is increased from 1.5 to 350 K (see Fig. 8 b). Another behavior is observed in the case of a non-centrosymmetric structure 186 where magnitude of distortion of neighboring oxygen octahedra is differed (see Fig. 7 b) that leads to appearance of various (uncompensated) local dipole moments. The influence of temperature factor to magnitude of local electric dipoles is shown in Fig. 10, a - d. The same difference in distortions of neighboring oxygen octahedra is observed for crystallographic positions 12k (SG 194) or 6c (SG 186) (see Fig.8, c).

It is necessary to note that the distortion of oxygen octahedra can be a reason of appearance of local electric dipoles for both centrosymmetric and non-centrosymmetric space groups. However, an unequal distortion of neighboring oxygen surroundings is origin of emerging of uncompensated

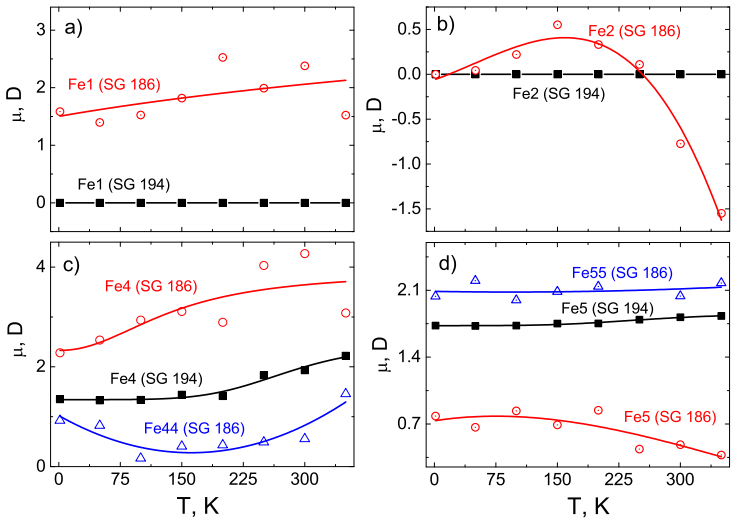

Figure 10: Temperature dependencies of electric dipoles as result of distortions of oxygen octahedrons around iron ions: Fe1 - (a); and Fe2 - (b); and Fe4 and Fe44 - (c); and Fe5 and Fe55 - (d).

local dipole moments that is the main reason of appearance of ferroelectric properties in hexaferrites.

3.4. Magnetic structure

The magnetic structure of $SrFe_{11.9}In_{0.1}O_{19}$ ferrite satisfies to the model proposed by Gorter [73] and it has ferrimagnetic order, where all magnetic moments of Fe^{3+} ions are oriented along c axis, which is easy magnetization axis. The magnetic moments of Fe^{3+} ions located in octahedral ($2a$ and $12k$) and bipyramidal ($2b$) oxygen surroundings are oriented in opposite to the magnetic moments of iron ions occupying positions ($4f_{IV}$ and $4f_{VI}$). As result, two ferromagnetic sublattices that directed in opposite direction make the ferrimagnetic structure. As was mentioned above, the main feature of neutron diffraction method is the direct study of magnetic structure of material. Neutron diffraction patterns have been measured in a wide temperature range from 1.5 to 350 K, which is well below the paramagnetic – ferrimagnetic phase transition temperature ($T_C \sim 670$ K) for a

$SrFe_{11.9}In_{0.1}O_{19}$ compound (see inset in Fig. 2). In Fig.4, the bottom row of vertical bars indicates the positions of diffraction peaks calculated by the Rietveld method for the magnetic structure of strontium hexaferrite. The absence of additional magnetic peaks on neutron diffraction patterns indicates that the wave vector of this ferrimagnetic structure: $\mathbf{k} = [0,\ 0,\ 0]$. As was mentioned above the unit cell has been refined in the framework both centrosymmetric ($P6_3/mmc$) and non-centrosymmetric ($P6_3mc$) space groups therefore magnetic moments have been also calculated separately for each space group. The temperature dependences of magnetic moments of Fe^{3+} ions in various crystallographic positions are shown in Fig.11, a and b. Values of magnetic moments in different crystallographic positions in the entire temperature range do not exceed the magnitude 5 μ_B peculiar to magnetic moment for Fe^{3+} that is indirect confirmation correctness of carried out refinements.

The total magnetic moment per formula unit of strontium ferrite ($SrFe_{12}O19$) with a centrosymmetric structure can be calculated with equation [74]:

$$M_{total}(T) = 1[m_{Fe1}(T)] + 1[m_{Fe2}(T)] - 2[m_{Fe3}(T)] - 2[m_{Fe4}(T)] + 6[m_{Fe5}(T)] \tag{6}$$

In the case non- centrosymmetric structure, the total magnetic moment was calculated as:

$$\begin{aligned} M_{total}(T) = 1[m_{Fe1}(T)] + 1[m_{Fe2}(T)] - 1[m_{Fe3}(T)] - 1[m_{Fe33}(T)] - \\ -1[m_{Fe4}(T)] - 1[m_{Fe44}(T)] + 3[m_{Fe5}(T)] + 3[m_{Fe55}(T)] \end{aligned} \tag{7}$$

where m_i is the magnetic moment of Fe^{3+} ion in the i-th sublattice.

Temperature dependences of the total magnetic moments are shown in Fig. 12. It is necessary to note that values of the total magnetic moments in the case both centrosymmetric and non-centrosymmetric structures, have insignificant difference of magnitudes each from other that does not allow to give the preference to one of them. Moreover, the general view of magnetic structure is comparable for both SG 194 and SG 186 and it is shown in insert Fig.12. The magnitude of the total magnetic moment has slightly less value than 20 μ_B per formula unit (f.un.) in the low-temperature region. It is due to the influence of diamagnetic In ions, which disrupts the exchange interaction between neighboring $Fe^{3+} - O - Fe^{3+}$ ions. The decrease of total magnetic moment is observed with increasing of the ambient temperature. Such behavior is a result of thermal magnons excitation, who decrease the total magnetic moment proportionally to their number [75].

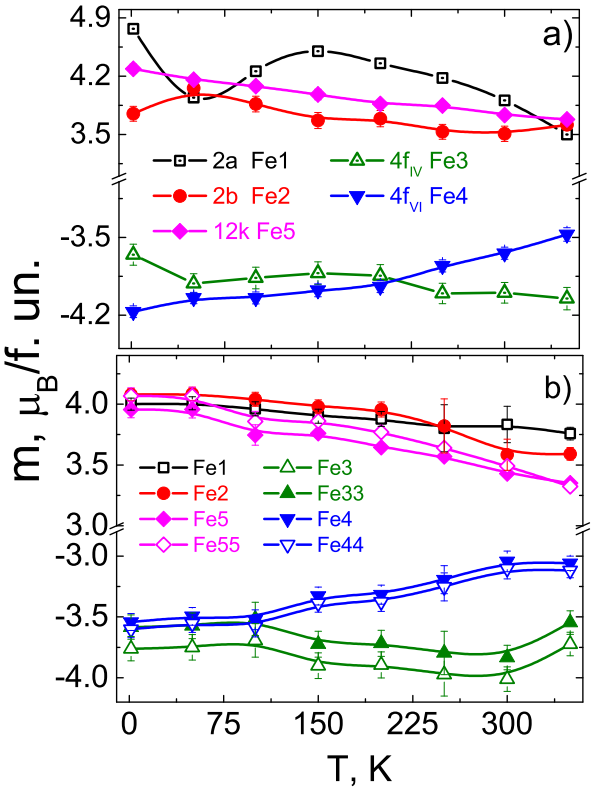

Figure 11: Temperature dependencies of local magnetic moments for suitable crystallographic positions for SG 194 - (a) and SG 186 - (b).

Conclusions

The observed decreasing of coercive field value with decreasing of ambient temperature has been explained by the fact that the saturation magnetization rises faster than the magnetic anisotropy constant. The divergence between FCW and ZFC temperature dependences of magnetizations indicates the presence of magnetically inhomogeneous system. The observed wide maximum on the ZFC curve at 55 K indicates the presence of size dispersion of

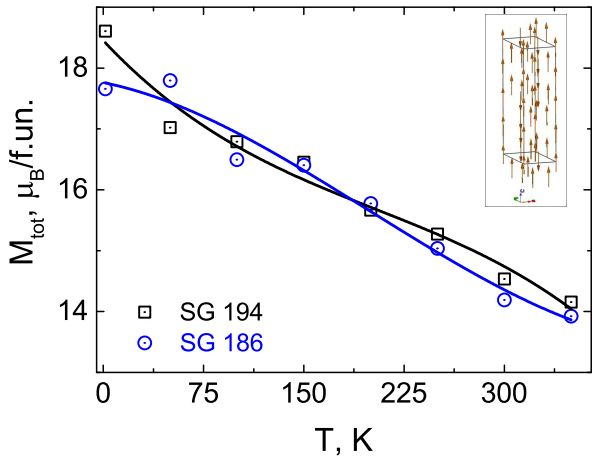

Figure 12: Temperature dependencies of total magnetic moments for SG 194 - (squares) and SG 186 - (circles). In inset: general view of magnetic structure of $SrFe_{11.9}In_{0.1}O_{19}$ compound is shown.

magnetic regions. The significant fraction of magnetic regions in the sample has average linear size ∼2.3 nm whereas the maximum linear size of magnetic domains achieves value ∼4.4 nm. It has been found out the appearance of ferroelectric properties in strontium ferrite partially substituted with diamagnetic In ions at room temperature. The fact that spontaneous polarization is observed in centrosymmetric unit cell, which contains inversion center, requires revising its crystal structure. With this purpose the crystal and magnetic structures of $SrFe_{11.9}In_{0.1}O_{19}$ compound have been investigated by neutron diffraction method in a wide temperature range from 1.5 to 350 K. Insignificant changes of lattice parameters have been observed in strontium hexaferrites in the temperature range from 1.5 to 150 K and explained by mutual rotations and tilts of oxygen polyhedra. In order to determine the real type of crystal structure of strontium ferrite, its structure was refined within the framework both centrosymmetric $P6_3/mmc$ (No. 194) and non-centrosymmetric $P6_3mc$ (No. 186) space groups. It was shown that the crystal structure of $SrFe_{11.9}In_{0.1}O_{19}$ compound can be described quite well by both space groups. However, less values figures of merit and the presence of ferroelectric properties allows to give preference to non-centrosymmetric $P6_3mc$ (No. 186) space group. Moreover, taking into account the presence of inversion center in the case of centrosymmetric unit cell the spontaneous

polarization will be absent in it because of compensation of local electric dipoles of adjacent polyhedra. On the contrary, in the non-centrosymmetric unit cell, the unequal distortion of neighboring oxygen octahedra is main reason of occurrence of spontaneous polarization. The magnetic structure of $SrFe_{11.9}In_{0.1}O_{19}$ compound is well described by the Gorter's model, according to which magnetic moments of all Fe^{3+} ions are ordered along hexagonal c axis, which is the axis of easy magnetization. The values of the total and local magnetic moments in various crystallographic positions in a wide temperature range were determined for unit cell described within the framework both centrosymmetric $P6_3/mmc$ (No. 194) and non-centrosymmetric $P6_3mc$ (No. 186) space groups.

Acknowledgements

The work was support by the Russian Science Foundation (Agreement No. 19-19-00694 of 06 May 2019). This project has received funding from the EU - H2020 research and innovation programme under grant agreement No 654360 having benefitted from the access provided by CSIC/ICMAB in Barcelona (ES) and by CEA/LLB in Paris (FR) within the framework of the NFFA – Europe Transnational Access Activity. (European grants to support the infrastructure of European centres of collective usage and mobile activity of researchers).

References

[1] B. Kaur, M. Bhat, F. Licci, R. Kumar, S.D. Kulkarni, P.A. Joy, K.K. Bamzai, P.N. Kotru, Modifications in magnetic anisotropy of M-type strontium hexaferrite crystals by swift heavy ion irradiation, *J. Magn. Magn. Mater.* **305** (2006) 392–402. doi:10.1016/j.jmmm.2006.01.110.

[2] L. A. Trusov, E. A. Gorbachev, V. A. Lebedev, A. E. Sleptsova, I. V. Roslyakov, E. S. Kozlyakova, A. V. Vasiliev, R. E. Dinnebier, M. Jansen, P. E. Kazin, Ca-Al double-substituted strontium hexaferrites with giant coercivity, *Chem. Commun.*, **54** (2018) 479–482. doi:10.1039/c7cc08675j.

[3] T. Tsutaoka, N. Koga, Magnetic phase transitions in substituted barium ferrites $BaFe_{12-x}(Ti_{0.5}Co_{0.5})_xO_{19}$ (x=0-5), *J. Magn. Magn. Mater.* **325** (2013) 36–41. doi:10.1016/j.jmmm.2012.07.050.

[4] B. T. Shirk, W. R. Buessem, Temperature Dependence of Ms and K1 of $BaFe_{12}O_{19}$ and $SrFe_{12}O_{19}$ Single Crystals, *J. Appl. Phys.* **40**(3) (1969) 1294–1296. https://doi.org/10.1063/1.1657636.

[5] M. N. Ashiq, A. S. Asi, S. Farooq, M. Najam-ul-Haq, S. Rehman, Magnetic and electrical properties of M-type nano-strontium hexaferrite prepared by sol-gel combustion method, *J. Magn. Magn. Mater.* **444** (2017) 426-431. doi.org/10.1016/j.jmmm.2017.08.065.

[6] N. Sapoletova, S. Kushnir, K. Ahn, S. Y. An, M. Choi, J. Y. Kim, Ch. Choi, W. Sungkwon, M-Zn (M = Sb, V, and Nb) Substituted Strontium Hexaferrites with Enhanced Saturation Magnetization for Permanent Magnet Applications *J. Magn.* **21**(3) (2016) 315–321. doi:10.4283/JMAG.2016.21.3.315.

[7] Ashima, S. Sanghi, A. Agarwal, Reetu, Rietveld refinement, electrical properties and magnetic characteristics of Ca-Sr substituted barium hexaferrites, *J. All. Comp.* **513** (2012) 436–444. doi:10.1016/j.jallcom.2011.10.071.

[8] R. C. Pullar, Hexagonal ferrites: A review of the synthesis, properties and applications of hexaferrite ceramics, *Progr. Mater. Science*, **57** (2012) 1191–1334. doi:10.1016/j.pmatsci.2012.04.001

[9] A. Awadallah, S.H. Mahmood, Y. Maswadeh, I. Bsoul, M. Awawdeh, Q.I. Mohaidat, H. Juwhari, Structural, magnetic, and Mossbauer spectroscopy of Cu substituted M-type hexaferrites, *Mater. Res. Bull.* **74** (2016) 192–201. doi:10.1016/j.materresbull.2015.10.034

[10] J. Mohammed, T. T. Carol, T., H.Y. Hafeez, D. Basandrai, G. R. Bhadu, S. K. Godara, S.B. Narang, A.K. Srivastava, Electromagnetic interference (EMI) shielding, microwave absorption, and optical sensing properties of BaM/CCTO composites in Ku-band, *Res. Phys.* **13** (2019) 102307 doi:10.1016/j.rinp.2019.102307

[11] A. T. Wise, J. Rocks, D. E. Laughlin, M. E. McHenry, S. D. Yoon, C. Vittoria, V. G. Harris, M-type barium hexaferrite synthesis and characterization for phase shifter applications, *J. Appl. Phys.* **109** (2011) 07E535(1-3). doi:10.1063/1.3559471

[12] V. Sharma, S. Kumari, B. K.Kuanr, Exchange-coupled hard-soft ferrites; A new microwave material, *J. All. Comp.*, **736** (2018) 266–275. doi:10.1016/j.jallcom.2017.11.113

[13] Y. Wang, Y. Liu, X. You, S. Liu, Ch. Wu, Q. Liu, H. Zhang, V. G.Harris, Crystallographically textured Zn2W-type barium hexaferrite for microwave and millimeter wave applications, *J. All. Comp.* **772** (2019) 1100–1104. doi:10.1016/j.jallcom.2018.09.087

[14] I. Ali, N. Shaheen, M.U.Islam, M. Irfan, M. N. Ashiq, M.A. Iqbal, A. Iftikhar, Study of electrical and dielectric behavior of Tb+3 substituted Y-type hexagonal ferrite, *J. All. Comp.* **617** (2014) 863–868. doi:10.1016/j.jallcom.2014.08.055

[15] V. G. Harris, A. Geiler, Y. Chen, S. D. Yoon, M. Wu, A. Yang, Zh. Chen, P. He, P. V. Parimi, X. Zuo, C. E. Patton, M. Abe, O. Acher, C. Vittoria, Recent advances in processing and applications of microwave ferrites, *J. Magn. Magn. Mater.* **321** (2009) 2035–2047. doi:10.1016/j.jmmm.2009.01.004

[16] S. D. Johnson, E. A. Patterson, J. Xing, S. Shin, S. B. Qadri, E. P. Gorzkowski, Design and Implementation of a Magnetic Press System for Creating Magnetically Oriented Barium Hexaferrite Pucks, *IEEE Trans. Magn.*, **55**(7) (2019) 1-6. doi:10.1109/TMAG.2019.2900241

[17] V. G. Harris, A. S. Sokolov, The Self-Biased Circulator: Ferrite Materials Design and Process Considerations, *J. Sup. Nov. Magn.* **32**(1) (2019) 97–108. doi:10.1007/s10948-018-4928-9

[18] V. G. Harris, Z. Chen, Y. Chen, S. Yoon, T. Sakai, A. Gieler, A. Yang, Y. He, Ba-Hexaferrite Films for Next Generation Microwave Devices (Invited), *J. Appl. Phys.* **99** (2006) 08M911(1–5). doi:10.1063/1.2165145

[19] S. Sugimoto, K. Haga, T. Kagotani, K. Inomata, Microwave absorption properties of Ba M-type ferrite prepared by a modified coprecipitation method, *J. Magn. Magn. Mater.* **290** (2005) 1188–1191. doi:10.1016/j.jmmm.2004.11.381

[20] F. M. M. Pereira, M. R. P. Santos, R. S. T. M. Sohn, J. S. Almeida, A. M. L. Medeiros, M. M. Costa, A. S. B. Sombra, Mag-

netic and dielectric properties of the M-type barium strontium hexaferrite ($Ba_xSr_{1-x}Fe_{12}O_{19}$) in the RF and microwave (MW) frequency range, *J. Mater. Sci. Mater. Electr.* **20**(5) (2009) 408–417. doi:10.1007/s10854-008-9744-8

[21] M. G.Vakhitov, D.S. Klygach, D.A. Vinnik, V.E. Zhivulin, N.S. Knyazev, Microwave properties of aluminum-substituted barium hexaferrite $BaFe_{12-x}Al_xO_{19}$ ceramics in the frequency range of 32-50 GHz, *J. All. Comp.* (2019) 152682 [in press]. doi:10.1016/j.jallcom.2019.152682

[22] H. Nikmanesh, S. Hoghoghifar, B. Hadi-Sichani, Study of the structural, magnetic, and microwave absorption properties of the simultaneous substitution of several cations in the barium hexaferrite structure, *J. All. Comp.* **775** (2019) 1101–1108. doi:10.1016/j.jallcom.2018.10.051

[23] V. Adelskold, X-ray studies on magneto-plumbite, $PbO * 6Fe_2O_3$ and other substances resembling beta-alumina, Na_2O $11Al_2O_3$, *Arkiv for Kemi Mineralogioch Geologi* **A 12**(29) (1938) 1–9. .

[24] K. -S. Moon, E.-S. Lim, Y.-M. Kang, Effect of Ca and La substitution on the structure and magnetic properties of M-type Sr-hexaferrites, *J. All. Comp.* **771** (2019) 350–355. doi:10.1016/j.jallcom.2018.08.306

[25] W. Zhang, Q. Zhu, R. Tang, H. Zhou, J. Zhang, J. Jiang, H. Yang, X. Su, Temperature dependent magnetic properties of conical magnetic structure M-type hexaferrites $BaFe_{10.2}Sc_{1.8}O_{19}$ and $SrFe_{10.2}Sc_{1.8}O_{19}$, *J. All. Comp.* **750** (2018) P. 368-374. doi:10.1016/j.jallcom.2018.03.260

[26] G. Tann, X. Chen, Structure and multiferroic properties of barium hexaferrite ceramics, *J. Magn. Magn. Mater.* **327** (2013) 87–90. doi:10.1016/j.jmmm.2012.09.047.

[27] G. Tan X. Chen, Synthesis, Structures, and Multiferroic Properties of Strontium Hexaferrite Ceramics, *J. Electr. Mater.* **42**(5) (2013) 906–911. doi:10.1007/s11664-012-2426-6.

[28] G. Tan, M. Wang, Multiferroic $PbFe_{12}O_{19}$ Ceramics, *J. Electrocer.* **26** (2011) 170–174. doi:10.1007/s10832-011-9641-z.

[29] V. G. Kostishyn, L.V. Panina, A.V. Timofeev, L.V. Kozhitov, A.N. Kovalev, A.K. Zyuzin, Dual ferroic properties of hexagonal ferrite ceramics $BaFe_{12}O_{19}$ and $SrFe_{12}O_{19}$ *J. Magn. Magn. Mater.* **400** (2016) 327–332. doi:10.1016/j.jmmm.2015.09.011.

[30] Y. Tokunaga, Y. Kaneko, D. Okuyama, S. Ishiwata, T. Arima, S. Wakimoto, K. Kakurai, Y. Taguchi, and Y. Tokura, Multiferroic M-type hexaferrites with a room-temperature conical state and magnetically controllable spin helicity, *Phys. Rev. Lett.* **105** (2010) 257201(1-4). doi:10.1103/PhysRevLett.105.257201.

[31] M. R. Sahoo, A. Barik, S. Kuila, S. Tiwary, P. N. Vishwakarma, Enhanced magnetoelectricity in bismuth substituted $SrFe_{12}O_{19}$ hexaferrite, *J. Appl. Phys.* **126** (2019) 074104(1–13) doi:10.1063/1.5095979

[32] S. Zare, H. Izadkhah, S. Somu, C. Vittoria, Magnetoelectric sensor excitations in hexaferrite slabs, *J. Appl. Phys.* **117** 2015) 214506 doi:10.1063/1.4922125

[33] G. Wang, S. Cao, Y. Cao, S. Hu, X. Wang, Z. Feng, B. Kang, Y. Chai, J. Zhang, W. Ren, Magnetic field controllable electric polarization in Y-type hexaferrite $Ba_{0.5}Sr_{1.5}Co_2Fe_{12}O_{22}$, *J. Appl. Phys.* **118** (2015) 094102(1–5). doi:10.1063/1.4929956

[34] K. Ebnabbasi, M. Mohebbi, C. Vittoria, Room temperature magnetoelectric effects in bulk poly-crystalline materials of M- and Z-type hexaferrites, *J. Appl. Phys.* **113** (2013) 17C703(1–3). doi:10.1063/1.4793606

[35] J. P. Martinez-Perez, A.M. Bolarin-Miro, F. Pedro-Garcia, C.A. Cortes-Escobedo, A. Barba-Pingarron, F. Sanchez-De Jesus, Magnetic and dielectric characterization of $xBiFeO_3 : (1-x)SrFe_{12}O_{19}$ multiferroic composites, *J. All. Comp.* **808** (2019) 151700(1–8). doi:10.1016/j.jallcom.2019.151700

[36] A. F. Ravinski, I.I. Makoed, K. Kokoshkevich, K.I. Yanushkevich, A.I. Galyas, V.V. Triguk, Magnetic properties and electron density distribution of $La_xBi_{1-x}FeO_3$, *Inorg. Mater.* **43** (2007) 860–865. doi:10.1134/S0020168507080080

[37] A. M. Balagurov, Scientific Reviews: High-Resolution Fourier Diffraction at the IBR-2 Reactor, *Neutron News* **16**(3) (2005) 8–12. doi:10.1080/10446830500454346.

[38] J. Rodriguez-Carvajal, Recent advances in magnetic structure determination by neutron powder diffraction, *Physica B* **192**(1-2) (1993) 55–69. doi:10.1016/0921-4526(93)90108-I.

[39] M. Jean, V. Nachbaur, J. Bran, J.M. Le Breton, Synthesis and characterization of $SrFe_{12}O_{19}$ powder obtained by hydrothermal process. *J. Alloy. Compd.* **496**(1-2), (2010) 306–312 doi:10.1016/j.jallcom.2010.02.002.

[40] M. Ghimire, S. Yoon, L. Wang, D. Neupane, J. Alam, S. R. Mishra, Influence of La content on magnetic properties of Cu doped M-type strontium hexaferrite: Structural, magnetic, and Mossbauer spectroscopy study, *J. Magn. Magn. Mater.*, **454** (2018) 110–120. doi:10.1016/j.jmmm.2018.01.062.

[41] A. Xia, C. Zuo, L. Zhang, C. Cao, Y. Deng, W. Xu, M. Xie, S. Ran, C. Jin, X. Liu, Magnetic properties, exchange coupling and novel stripe domains in bulk $SrFe_{12}O_{19}/(Ni, Zn)Fe_2O_4$ composites, *J. Phys. D: Appl. Phys.* **47**(41), (2014) 415004–415014. doi:10.1088/0022-3727/47/41/415004.

[42] Z. Yang, C.S. Wang, X.H. Li, H.X. Zeng (Zn, Ni, Ti) substituted barium ferrite particles with improved temperature coefficient of coercivity, *Materials Science and Engineering* **B 90**(1-2) (2002) 142–145. doi:10.1016/S0921-5107(01)00925-4.

[43] J. Wang, F. Zhao, W. Wu, G.-M. Zhao Unusual temperature dependence of the magnetic anisotropy constant in barium ferrite $BaFe_{12}O_{19}$ *J. Appl. Phys.* **110** (2011) 096107(1–3). doi:10.1063/1.3657851.

[44] N. S. Akulov, Uber den Verlauf der Magnetisierungskurve in starken Feldern, *Ztschr. Physik*, **69**(11-12), (1931) 822–831.

[45] X. Batlle, X. Obradors, J. Rodriguez-Carvajal, M. Pernet, M. V. Cabanas, M. Vallet, Cation distribution and intrinsic magnetic properties of Co-Ti-doped M-type barium ferrite, *J. Appl. Phys.*, **70**(3) (1991) 1614–1623. doi:10.1063/1.349526.

[46] H. Hauser, D.C. Jiles, Y. Melikhov, L.Li, R. Grossinger, An approach to modeling the dependence of magnetization on magnetic field in the high field regime *J. Magn. Magn. Mater.* **300** (2006) 273–283 doi:10.1016/j.jmmm.2005.05.017.

[47] Q. Li, J. Song, M. Saura-Muzquiz, F. Besenbacher, M. Christensen, M. Dong, Magnetic Properties of Strontium Hexaferrite Nanostructures Measured with Magnetic Force Microscopy, *Scient. Rep.* **6** (2016) 25985(1–7). doi:10.1038/srep25985.

[48] D. L. Kunwar, D. Neupane, J. N. Dahal, S. R. Mishra, Structural, Magnetic, and Electrical Properties of RE Doped $Sr_{0.82}RE_{0.18}Fe_{12-x}Al_xO_{19}$ (RE = Gd, Pr, Sm) Compound, *Adv. Mater. Phys. Chem.* **9** (2019) 175–198. doi:10.4236/ampc.2019.99014

[49] S.S. Veisi, M.Yousefi, M.M.Amini, A.R.Shakeri, M.Bagherzadeh, Magnetic and microwave absorption properties of Cu/Zr doped M-type Ba/Sr hexaferrites prepared via sol-gel auto-combustion method, *J. All. Comp.* **773** (2019) 1187–1194. doi:10.1016/j.jallcom.2018.09.189

[50] Z. F. Zi, Y.P. Sun, X.B. Zhu, Z.R. Yang, J.M. Dai, W.H. Song, Structural and magnetic properties of $SrFe_{12}O_{19}$ hexaferrite synthesized by a modified chemical co-precipitation method. *J. Magn. Magn. Mater.* **320** (2008) 2746–2751. doi:10.1016/j.jmmm.2008.06.009

[51] P. Sivakumar, L. Shani, Y. Yeshurun, A. Shaulov, A. Gedanken, Facile sonochemical preparation and magnetic properties of strontium hexaferrite ($SrFe_{12}O_{19}$) nanoparticles, *J. Mater. Sci: Mater. Electron* **27**(6) (2016) 5707–5714. doi:10.1007/s10854-016-4482-9.

[52] E. V. Pashkova, E.D. Solovyova, T.V. Kolodiazhnyi, V.P. Ivanitskii, A.G. Belous, Effect of heat treatment on the phase composition, structure and magnetic properties of M-type barium hexaferrite, *J. Magn. Magn. Mater.* **368** (2014) 1–7. doi:10.1016/j.jmmm.2014.04.068.

[53] E. C. Stoner, E.P. Wohlfarth, A mechanism of magnetic hysteresis in heterogeneous alloys, *IEEE Trans. Magn.*, **27**(4) (1991) 3475–3518. doi:10.1109/TMAG.1991.1183750.

[54] E. C. Stoner, E. P. Wohlfarth, A Mechanism of Magnetic Hysteresis in Heterogeneous Alloys, *Phil. Trans. Roy. Soc.*, **240**(826) (1948) 599–642.

[55] R. Topkaya, Effect of composition and temperature on the magnetic properties of $BaBi_xLa_xFe_{(12-2x)}O_{19}$ ($0.0 < x < 0.2$) hexaferrites, *Appl. Phys.*, **A 123** (2017) 488(1–8). doi:10.1007/s00339-017-1115-y.

[56] M. A. Almessiere, Y. Slimani, M. Sertkol, M. Nawaz, A. Baykal, I. Ercan, The impact of Zr substituted Sr hexaferrite: Investigation on structure, optic and magnetic properties, *Res. Phys* **13** (2019) 102244(1–9). doi:10.1016/j.rinp.2019.102244

[57] M. A. Almessiere, Y. Slimani, N. A. Tashkandi, H. Gungunes, M. Sertkol, M. Nawaz, S. Ali, A. Baykal, I. Ercan, Tailored microstructures, optical and magnetic qualities of strontium hexaferrites: Consequence of Tm^{3+} and Tb^{3+} ions Co-substitution, *Ceram. Intern.* **45**(17) (2019) 21385–21394. doi:10.1016/j.ceramint.2019.07.126

[58] A. H. El-Sayed, O. M. Hemeda, A. Tawfik, M. A. Hamad, Remarkable magnetic enhancement of type-M hexaferrite of barium in polystyrene polymer, *AIP Advanc.* **5** (2015) 107131(1–6). doi:10.1063/1.4934790

[59] R. C. Pullar, Hexagonal ferrites: A review of the synthesis, properties and applications of hexaferrite ceramics, *Progr. Mater. Science*, **57** (2012) 1191–1334. doi:10.1016/j.pmatsci.2012.04.001.

[60] S. V. Trukhanov, A.V. Trukhanov, V.A. Turchenko, V.G. Kostishyn, L.V. Panina, I.S. Kazakevich, A.M. Balagurov, Structure and magnetic properties of $BaFe_{11.9}In_{0.1}O_{19}$ hexaferrite in a wide temperature range, *J. All. Comp.* **689** (2016) 383–393. doi:10.1016/j.jallcom.2016.07.309.

[61] A. V. Trukhanov, V.G. Kostishyn, L.V. Panina, V.V. Korovushkin, V.A. Turchenko, P. Thakur, A. Thakur, Y. Yang, D.A. Vinnik, E.S. Yakovenko, L. Yu. Matzui, E.L. Trukhanova, S.V. Trukhanov, Control of electromagnetic properties in substituted M-type hexagonal ferrites, *J. All. Comp.* **754** (2018) 247–256. doi:10.1016/j.jallcom.2018.04.150.

[62] R. W. Chantrell, N. S. Walmsley, J. Gore, M. Maylin, Theoretical studies of the field-cooled and zero-field cooled magnetization of interacting fine particles, *J. Appl. Phys.*, **85** (1999) 4340–4342. doi:10.1063/1.370361.

[63] K. Binder, A. P. Young, Spin glasses: experimental facts, theoretical concepts, and open questions, *Rev. Modern Phys.*, **58**(4) (1986) 802–976. doi:10.1103/RevModPhys.58.801.

[64] W. T. Coffey, D. S. F. Crothers, J. L. Dormann, L. J. Geoghegan, Yu. P. Kalmykov, J. T. Waldron, A. W. Wickstead, The effect of an oblique magnetic field on the superparamagnetic relaxation time, *J. Magn. Magn. Mater.*, **145**(3) (1995) L263-L267. doi:10.1016/0304-8853(94)00863-9.

[65] S. Morup, D. E. Madsen, C. Fradsen, C. R. H. Bahl, M. F. Hansen, Experimental and theoretical studies of nanoparticles of antiferromagnetic materials, *J. Phys.: Condens. Matter.*, **19** (2007) 213202(1-31). doi:10.1088/0953-8984/19/21/213202.

[66] E. F. Kneller, F. E. Luborsky, Particle Size Dependence of Coercivity and Remanence of Single-Domain Particles, *J. Appl. Phys.*, **34**(3) (1963) 656–658. doi:10.1063/1.1729324.

[67] L. Ajroudi, N. Mliki, L. Bessais, V. Madigou, S. Villain, C. Leroux, Magnetic, electric and thermal properties of cobalt ferrite nanoparticles *Mater. Research Bulletin, Elsevier*, **59** (2014) 49–58 doi:10.1016/j.materresbull.2014.06.029.

[68] C. P. Bean, J. D. Livingston, Superparamagnetism, *J. Appl. Phys.*, **30**(4) (1959) S120–S129. doi:10.1063/1.2185850.

[69] A. S. Mikheykin, E. S. Zhukova, V. I. Torgashev, A. G. Razumnaya, Y. I. Yuzyuk, B. P. Gorshunov, A. S. Prokhorov, A. E. Sashin, A. A. Bush, M. Dressel, Lattice anharmonicity and polar soft mode in ferrimagnetic M-type hexaferrite $BaFe_{12}O_{19}$ single crystal, *Eur. Phys. J. B*, **87** (2014) 232(1–9). doi:10.1140/epjb/e2014-50329-4.

[70] V. Turchenko, A. Trukhanov, S. Trukhanov, M. Balasoiu, N. Lupu, Correlation of crystalline and magnetic structures of barium ferrites withdual ferroic properties, *J. Magn. Magn. Mater.*, **477** (2019) 9–16. doi:10.1016/j.jmmm.2018.12.101.

[71] S. V. Trukhanov, A. V. Trukhanov, V .A. Turchenko, An. V. Trukhanov, E. L. Trukhanova, D. I. Tishkevich, V. M. Ivanov, T. I. Zubar, M. Salem,

V. G. Kostishyn, L. V. Panina, D. A. Vinnik, S. A. Gudkova, Polarization origin and iron positions in indium doped barium hexaferrites, *Ceramics International*, **44** (2018) 290–300. doi:10.1016/j.ceramint.2017.09.172.

[72] V. Turchenko, A. Trukhanov, S. Trukhanov, I. Bobrikov, A. M. Balagurov, Features of crystal and magnetic structures of solid solutions $BaFe_{12-x}D_xO_{19}$ (D = Al^{3+} and In^{3+}; x = 0.1) in a wide temperature range, *Eur. Phys. J. Plus*, **131** (2016) 82(1–10). doi:10.1140/epjp/i2016-16082-x.

[73] E. Gorter, Saturation magnetization of some ferrimagnetic oxides with hexagonal crystal structures, *Proc. IEE B: Radio and Electr. Engin.*, **104**(5) (1957) 255–260. doi:10.1049/pi-b-1.1957.0042.

[74] J. Smit, H.P.J. Wijn, Ferrites: physical properties of ferrimagnetic oxides in relation to their technical application, *Wiley-Inter Science, New York*, 1959.

[75] C. Kittel, Introduction to Solid State Physics, *J. Wiley and Sons, New York*, 1996.

Table 2: Crystal structure parameters, figures of merit and atomic positions refined in the framework of centrocymmetric SG $P6_3/mmc$ (No. 194) with the Rietveld method for different temperatures. Atoms are located in positions: Sr (2d) (2/3, 1/3, 1/4), Fe1 (2a) (0, 0, 0); Fe2 (2b) (0, 0, 1/4); (Fe/In)3 ($4f_{IV}$) (1/3, 2/3, z); (Fe/In)4 ($4f_{VI}$) (1/3, 2/3, z); (Fe/In)5 (12k) (x, 2x, z); O1 (4e) (0, 0, z); O2 (4f) (1/3, 2/3, z); O3 (6h) (x, 2x, 1/4); O4 (12k) (x, 2x, z); O5 (12k) (x, 2x, z).

Parameters	Temperature				
	1.5 K	100 K	200 K	300 K	740 K
a, ($\AA$)	5.8737(1)	5.8737(1)	5.8753(2)	5.8786(2)	5.8999(1)
c, ($\AA$)	22.9810(7)	22.9931(7)	23.0161(7)	23.0435(8)	23.1818(2)
V, ($\AA^3$)	686.64(3)	686.99(3)	688.06(3)	689.64(4)	698.83(1)
Fe3/In ($4f_{IV}$)					
z	0.0297(6)	0.0310(5)	0.0311(5)	0.0309(6)	0.0282(1)
Fe4/In ($4f_{VI}$)					
z	0.1927(5)	0.1919(5)	0.1924(5)	0.1933(5)	0.1895(1)
Fe5/In ($12k$)					
x	0.1844(11)	0.1835(11)	0.1843(12)	0.1851(12)	0.1672(3)
z	-0.1088(1)	-0.1087(1)	-0.1088(2)	-0.1089(2)	-0.1089(4)
O1 ($4e$)					
z	0.1439(6)	0.1440(6)	0.1437(6)	0.1439(7)	0.1514(2)
O2 ($4f$)					
z	-0.0399(7)	-0.0382(7)	-0.0377(7)	-0.0372(7)	-0.0555(2)
O3 ($6h$)					
x	0.1813(46)	0.1838(41)	0.1811(45)	0.1710(48)	0.1833(8)
O4 ($12k$)					
x	0.1636(27)	0.1622(26)	0.1624(26)	0.1649(27)	0.1577(6)
z	0.0544(3)	0.0545(3)	0.0549(3)	0.0554(3)	0.0534(9)
O5 ($12k$)					
x	0.4948(25)	0.4952(25)	0.4951(26)	0.4940(27)	0.5049
z	0.1539(3)	0.1540(3)	0.1539(3)	0.1536(3)	0.1506(7)
R_{wp}, %	5.58	5.60	5.90	6.12	5.27
R_{exp}, %	3.89	3.91	3.92	3.97	3.40
R_B, %	3.48	3.40	3.82	4.59	10.7
R_{Mag}, %	4.09	3.74	4.58	5.45	–
χ^2	2.05	2.05	2.26	2.38	2.41

Table 3: Crystal structure parameters, figures of merit and atomic positions refined in the framework of centrocymmetric SG $P6_3mc$ (No. 186) with the Rietveld method for different temperatures. Atoms are located in positions: Sr (2b) (2/3, 1/3, z); Fe1 (2a) (0, 0, z); Fe2 (2a) (0, 0, z); (Fe/In)3 (2b) (1/3, 2/3, z); (Fe/In)33 (2b) (1/3, 2/3, z); (Fe/In)4 (2b) (1/3, 2/3, z); (Fe/In)44 (2b) (1/3, 2/3, z); (Fe/In)5 (6c) (x, 2x, z); (Fe/In)55 (6c) (x, 2x, z); O1 (2a) (0, 0, z); O11 (2a) (0, 0, z); O2 (2b) (1/3, 2/3, z); O22 (2b) (1/3, 2/3, z); O3 (6c) (x, 2x, z); O4 (6c) (x, 2x, z); O44 (6c) (x, 2x, z); O5 (6c) (x, 2x, z); O55 (6c) (x, 2x, z).

Parameters	Temperature			
	1.5 K	100 K	200 K	300 K
a, ($\AA$)	5.8737(1)	5.8737(1)	5.8753(2)	5.8786(2)
c, ($\AA$)	22.9810(7)	22.9931(7)	23.0161(7)	23.0435(8)
V, ($\AA^3$)	686.64(3)	686.99(3)	688.06(3)	689.64(4)
Sr (2*b*)				
z	0.2661(13)	0.2683(33)	0.2645(18)	0.2637(14)
Fe1 (2*a*)				
z	-0.0054(17)	0.0002(36)	-0.0089(17)	-0.0112(16)
Fe2 (2*a*)				
z	0.2468(19)	0.2516(40)	0.2472(22)	0.2460(20)
Fe3/In (2*b*)				
z	0.0252(12)	0.0284(22)	0.0235(19)	0.0251(21)
Fe33/In (2*b*)				
z	0.4634(16)	0.4661(25)	0.4604(24)	0.4584(22)
Fe4/In (2*b*)				
z	0.1993(8)	0.2003(29)	0.1969(18)	0.1952(24)
Fe44/In (2*b*)				
z	0.3099(11)	0.3122(19)	0.3066(19)	0.3033(23)
Fe5/In (6*c*)				
x	0.1754(32)	0.1752(33)	0.1761(34)	0.1791(45)
z	0.8877(8)	0.8911(24)	0.8875(12)	0.8876(10)
Fe55/In (6*c*)				
x	0.8281(30)	0.8269(36)	0.8257(29)	0.8233(41)
z	0.1084(7)	0.1108(23)	0.1083(14)	0.1092(11)
O1 (2*a*)				
z	0.1520(20)	0.1547(30)	0.1506(28)	0.1546(37)
O11 (2*a*)				
z	0.3416(19)	0.3468(41)	0.3404(28)	0.3441(42)
O2 (2*b*)				
z	0.93754	0.94237(225)	0.93754(0)	0.94465(257)
O22 (2*b*)				
z	0.5310(24)	0.5327(25)	0.5289(23)	0.5279
O3 (6*c*)				
x	0.1864(40)	0.1861	0.1839(51)	0.1738(72)
z	0.2500	0.2559(36)	0.2515(16)	0.2527(9)
O4 (6*c*)				
x	0.1803(47)	0.1805(54)	0.1818(49)	0.1774(63)
z	0.0452	0.0504(42)	0.0463(8)	0.0452
O44 (6*c*)				
x	0.1416(41)	0.1421	0.1433(46)	0.1446(48)
z	0.4355(7)	0.4410(48)	0.4358	0.4339(9)
O5 (6*c*)				
x	0.4625(38)	0.4616(51)	0.4635(48)	0.4639(44)
z	0.1581	0.1580	0.1561(11)	0.1577(11)
O55 (6*c*)				
x	0.5018(58)	0.5074(61)	0.5003(64)	0.4951(75)
z	0.3474(7)	0.3489(10)	0.3464	0.3465
R_{wp}, %	4.73	4.94	5.17	5.25
R_{exp}, %	3.87	3.88	3.90	3.94
R_B, %	1.60	1.69	2.04	2.57
R_{Mag}, %	1.75	1.80	2.51	3.23
χ^2	1.49	1.62	1.76	1.77